

**Out-of-plane instability and electron-phonon contribution to  $s$ - and  $d$ -wave pairing in high-temperature superconductors; LDA linear-response calculation for doped  $\text{CaCuO}_2$  and a generic tight-binding model.**

O. K. Andersen, S. Y. Savrasov, O. Jepsen, and A.I.Lichtenstein

*Max-Planck Institut für Festkörperforschung, 70569 Stuttgart, Germany*

*The equilibrium structure, energy bands, phonon dispersions, and  $s$ - and  $d$ -channel electron-phonon interactions (EPIs) are calculated for the infinite-layer superconductor  $\text{CaCuO}_2$  doped with 0.24 holes per  $\text{CuO}_2$ . The LDA and the linear-response full-potential LMTO method were used. In the equilibrium structure, oxygen is found to buckle slightly out of the plane and, as a result, the characters of the energy bands near  $\epsilon_F$  are found to be similar to those of other optimally doped HTSCs. For the EPI we find  $\lambda_s \sim 0.4$ , in accord with previous LDA calculations for  $\text{YBa}_2\text{Cu}_3\text{O}_7$ . This supports the common belief that the EPI mechanism alone is insufficient to explain HTSC.  $\lambda_{x^2-y^2}$  is found to be positive and nearly as large as  $\lambda_s$ . This is surprising and indicates that the EPI could enhance some other  $d$ -wave pairing mechanism. Like in  $\text{YBa}_2\text{Cu}_3\text{O}_7$ , the buckling modes contribute significantly to the EPI, although these contributions are proportional to the static buckling and would vanish for flat planes. These numerical results can be understood from a generic tight-binding model originally derived from the LDA bands of  $\text{YBa}_2\text{Cu}_3\text{O}_7$ . In the future, the role of anharmonicity of the buckling-modes and the influence of the spin-fluctuations should be investigated.*

*PACS numbers: 74.72.Jt, 74.25.Kc, 63.20.Kr*

## 1. INTRODUCTION

The mechanism of high-temperature superconductivity in hole-doped  $\text{CuO}_2$  materials remains a subject of vivid debate.<sup>1</sup> The Coulomb repulsion between the electrons is poorly screened, at least for low doping levels, and it may be responsible for the pairing.<sup>2</sup> This is supported by experimental evidence that the symmetry of the paired state is  $d_{x^2-y^2}$  with lobes in the direction of the CuO-bond. Nevertheless, the results of Hubbard- and  $t$ - $J$ -model calculations using realistic parameters lead to a suspicion that something more than the Coulomb repulsion is needed.<sup>2</sup> A large amount of experimental data such as superconductivity-induced phonon renormalizations,<sup>3</sup> a large isotope effect away from optimal doping,<sup>4</sup> and phonon-related features in the tunnelling spectra<sup>5</sup> show effects of the electron-phonon interaction (EPI). It is therefore of interest to investigate whether the EPI, which gives a pair-interaction,  $V(\mathbf{k}, \mathbf{k}') \propto -|g(\mathbf{k}, \mathbf{k}')|^2$ , which is always negative (attractive), could support  $d_{x^2-y^2}$ -wave pairing with a gap-anisotropy like  $\Delta(\mathbf{k}) \propto \cos(ak_x) - \cos(ak_y)$ . For this to occur,  $|g(\mathbf{k}, \mathbf{k}')|^2$  must be large when  $\Delta(\mathbf{k})$  and  $\Delta(\mathbf{k}')$  have the same sign, and small when they have opposite signs. Such an investigation is the main topic of the present paper.

We first report *ab initio* local density-functional (LDA) calculations of the crystal, electronic, and phononic structure, and of the  $s$ - and  $d$ -channel EPIs for the infinite-layer compound  $\text{CaCuO}_2$ . Unfortunately, no single-crystal measurements exist for an infinite-layer HTSC, and the ceramic samples for which a  $T_c$  of 110K was reported<sup>6</sup> may be phase impure.<sup>7</sup> However, the infinite-layer structure is uniquely simple for theoretical studies and high-temperature superconductivity is generally believed to take place in  $\text{CuO}_2$  planes. As we shall see, also the LDA electronic structure of this material, properly relaxed, is very similar to that of the stoichiometrically doped, well-characterized HTSC,  $\text{YBa}_2\text{Cu}_3\text{O}_7$ . Our calculations are for 24 per cent hole-doped  $\text{CaCuO}_2$  with the hole charge being neutralized by a homogeneous, negative background charge. We have chosen a doping of 0.24 holes per  $\text{CuO}_2$  because this places the Fermi level at the uppermost saddle-point in the LDA band structure, and because it agrees with the experimental (average) doping level.

In the second part of the paper we present analytical low-energy bands, originally derived from LDA calculations for  $\text{YBa}_2\text{Cu}_3\text{O}_7$ ,<sup>8</sup> and derive the EPI for the buckling-mode. This tight-binding model has previously<sup>9</sup> been used to explain the in-plane dispersion of the inter-plane hopping integral  $t_\perp(\mathbf{k}_\parallel)$ , which is a crucial ingredient of the inter-plane tunnelling model of HTSC.<sup>11</sup> When augmented with a mean-field treatment of the Coulomb repulsion  $U$  between two holes in the same Cu  $d_{x^2-y^2}$  orbital, the model has

## Out-of-plane instability and electron-phonon contribution to ...

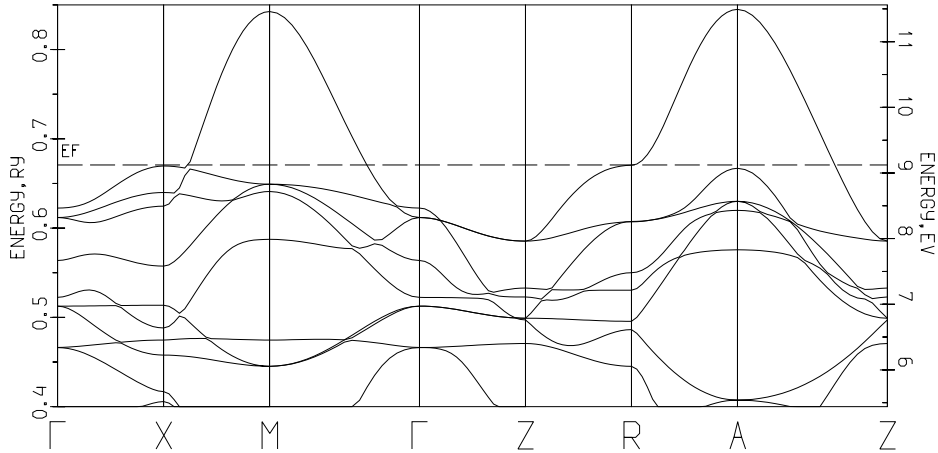


Fig. 1. Band structure of doped  $\text{CaCuO}_2$  with flat planes.

correctly predicted the value of the inter-plane exchange coupling  $J_{\perp}$ .<sup>10</sup> In the present paper we consider the EPI in optimally and overdoped HTSCs and shall assume that  $U$  is screened completely. We shall derive an analytical expression for the coupling  $g(\mathbf{k}, \mathbf{k} + \mathbf{q})$  of the electrons to the buckling mode for a single plane and show that, for this mode,  $\lambda$  for  $d_{x^2-y^2}$ -wave pairing is positive definite. The analytical tight-binding model should also be useful for further studies.

## 2. LDA CALCULATIONS FOR $\text{CaCuO}_2$

### 2.1. Energy bands and equilibrium structure.

In this section we discuss the electronic energy bands and the equilibrium structure calculated with our full-potential linear-muffin-tin-orbital (LMTO) method. The bands presented in Fig. 1 agree in detail with those of previous calculations,<sup>12</sup> and they hardly change upon hole doping by 10 per cent, except for a downwards shift of the Fermi energy to the uppermost van Hove singularity (at R) as shown in the figure. The Fermi surface (FS) for the doped compound (see Fig. 4a) has a square (10)-oriented cross-section with the  $\Gamma\text{XM}$ -plane ( $k_z=0$ ) and a (11)-oriented cross section with the  $\text{ZRA}$ -plane ( $k_z=\frac{\pi}{c}$ ).

Although the band structure in Fig. 1 has antibonding in-plane  $pd\sigma$ -character ( $\text{O}_x\text{-Cu}_{x^2-y^2}\text{-O}_y$ ), like for all  $\text{CuO}_2$ -HTSCs, at and above  $\epsilon_F$ , there are strong atypical features just below  $\epsilon_F$ : First of all, the uppermost band at X is an antibonding out-of-plane  $pd\pi$  band [the  $\text{O}_z\text{-Cu}_{xz}$  band at  $(\frac{\pi}{a}, 0, 0)$  and the  $\text{O}_z\text{-Cu}_{yz}$  band at  $(0, \frac{\pi}{a}, 0)$ ], whereas at R [ $(\frac{\pi}{a}, 0, \frac{\pi}{c})$  and  $(0, \frac{\pi}{a}, \frac{\pi}{c})$ ] the uppermost band is the usual  $pd\sigma$ -band. This is due to a relatively strong

dispersion,  $2t_{\perp}^{\pi}(\mathbf{k}_{\parallel}) \cos ck_z$ , of the  $pd\pi$  band in the  $z$ -direction, a dispersion which is opposite to that,  $-2t_{\perp}^{\sigma}(\mathbf{k}_{\parallel}) \cos ck_z$ , of the  $pd\sigma$  band. Secondly, near A the top of the antibonding in-plane  $pd\pi$  band ( $O_y$ -Cu<sub>xy</sub>- $O_x$ ) nearly reaches  $\epsilon_F$ .

Our total-energy calculations however predict that this infinite-layer structure is unstable with respect to the  $\mathbf{q}=0$  oxygen out-of-phase buckling mode ( $B_{2u}$ ). We have performed frozen-phonon calculations for both undoped and doped compounds and with both experimental and theoretical lattice parameters. The results are shown in Fig. 2. We see that a double-well potential exists for such buckling motions, when the system is doped. The minimum is at  $5^\circ$  if we use the experimental values:  $a=7.297$  a.u. and  $c/a=0.829$ , and at  $7^\circ$  if we use our theoretically determined values:  $a=7.112$  a.u. and  $c/a=0.895$ . Note that  $YBa_2Cu_3O_7$  has a  $7^\circ$  static in-phase dimpling of the Cu-O planes, both experimentally and theoretically.

The buckling reduces the in-plane  $t_{z,xz}=t_{z,yz}$  and  $t_{y,xy}=t_{x,xy}$  hopping integrals and thereby causes the tops of the out-of-plane and in-plane  $pd\pi$  bands to move well below  $\epsilon_F$ . For the theoretically stable structure, our bands in Fig. 3 and Fermi-surface cross sections in Fig. 4b are similar to those of other cuprates. Comparing in detail with the calculated FS of  $YBa_2Cu_3O_7$ ,<sup>8</sup> where the dimple causes the saddlepoint at the Fermi level (that of the odd plane band) to be bifurcated by  $\Delta k$  to the positions  $(\frac{\pi}{a} \pm \Delta k, 0, 0)$ , we see that the saddlepoint at the Fermi level in  $CaCuO_2$  is *not* bifurcated away from R  $(\frac{\pi}{a}, 0, \frac{\pi}{c})$ . The saddlepoints well below  $\epsilon_F$  (that of the even plane band in  $YBa_2Cu_3O_7$  and that for  $k_z=0$  in  $CaCuO_2$ ) *are* however bifurcated away from X in both materials. (The difference between the saddlepoints at  $k_z=\frac{\pi}{c}$  and  $k_z=0$  in  $CaCuO_2$  is due to the opposite  $k_z$ -dispersions of the  $pd\sigma$  and  $pd\pi$  bands.)

By comparison of the FS cross-sections in Figs 4a and b, we see that the static buckle squares up the (10)-oriented cross sections and thus creates *large, flat* (100)- and (010)-oriented pieces on the FS, centered near respectively  $(\frac{5\pi}{6a}, 0, 0)$  and  $(0, \frac{5\pi}{6a}, 0)$ .

The calculated instability suggests that out-of-plane buckling occurs generally in such materials when the Fermi level is lowered to the top of the  $pd\pi$  bands. Inclusion of the Coulomb correlations, would presumably cause such instabilities to occur at lower doping levels than we predict with the LDA because, in a mean-field treatment, the energy of the majority-spin Cu  $d_{x^2-y^2}$  orbital is lowered. The striped anti-ferromagnetic low-temperature-tetragonal (AF-LTT) phases recently found by neutron scattering in  $\frac{1}{8}$ -doped  $La_2CuO_4$ <sup>13</sup> and the local buckling instabilities found in 15 per cent doped  $La_2CuO_4$  by EXAFS<sup>14</sup> are presumably examples of this. Only when pinned,

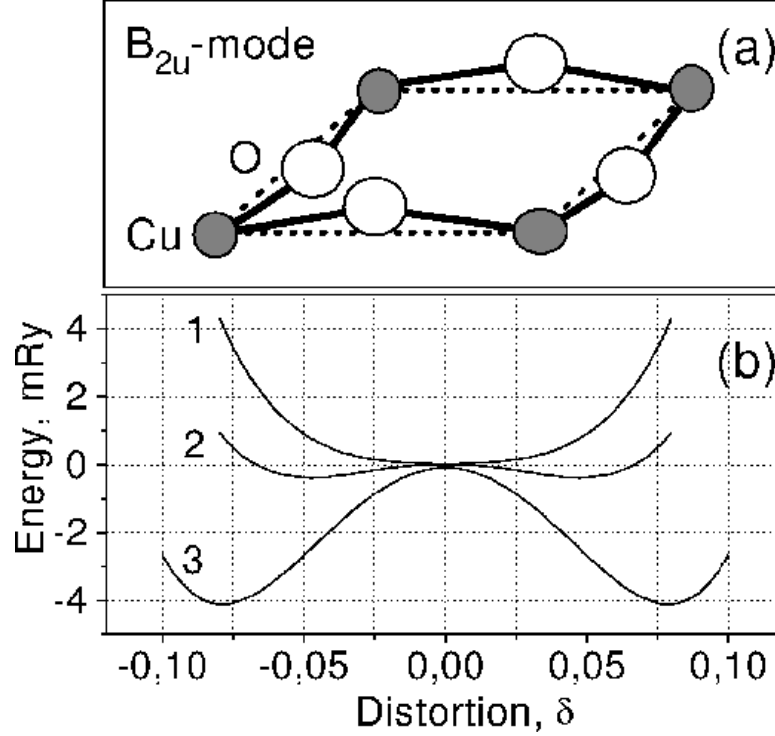


Fig. 2. (a) Unstable  $B_{2u}$  optical mode involving out-of-plane and out-of-phase displacements of oxygen atoms. (b) Change in the total energy associated with the  $B_{2u}$  mode. Curve 1 corresponds to the undoped compound calculated with the experimental lattice constants  $a_{exp}$  and  $c_{exp}$ . Curve 2: Doped compound with  $a_{exp}$ ,  $c_{exp}$ . Curve 3: Doped compound with calculated lattice constants.

do the AF stripes seem to be detrimental to superconductivity.

## 2.2. Phonon spectrum

We now present the phonon dispersions calculated for the doped compound. We use newly developed linear-response full-potential LMTO method<sup>15</sup> whose accuracy was proven on lattice-dynamical, superconducting, and transport properties for a large variety of metals.<sup>16</sup> The theoretical lattice constants were used in this calculation since the shallowness of the  $B_{2u}$ -well calculated with the experimental parameters casts serious doubts on the validity of the harmonic approximation. The technical details of this calculation can be found elsewhere.<sup>17</sup>

From the calculated phonon dispersions in Fig. 5, we first notice that the structure is stable. Secondly, we notice that a low frequency (1.8 THz)

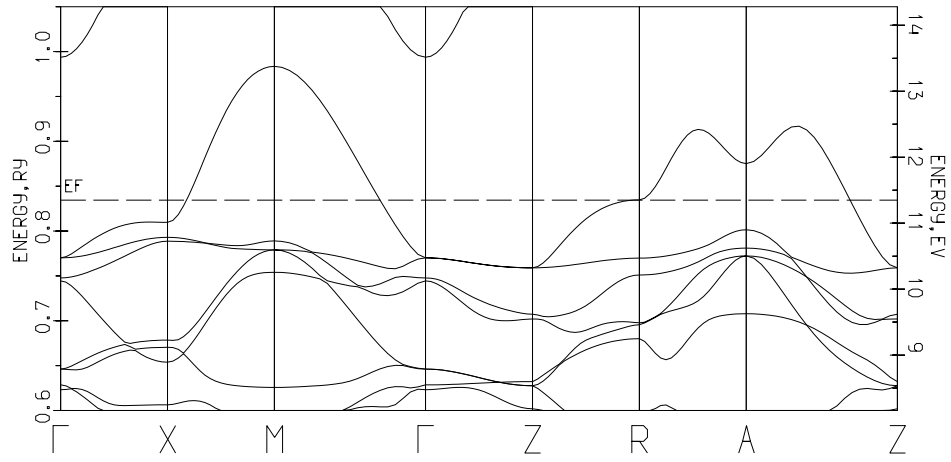


Fig. 3. Band structure of doped  $\text{CaCuO}_2$  with buckled planes.

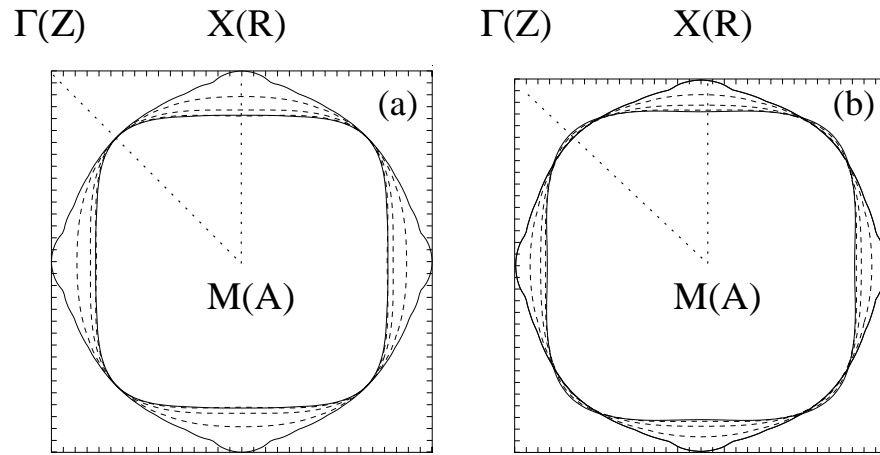


Fig. 4. Fermi surface cross sections of doped  $\text{CaCuO}_2$  with flat (a) and buckled (b) planes. The (10)-oriented cross section is with the  $\Gamma XM$  plane while (11)-oriented cross section is with the  $ZRA$  -plane. The dashed lines show intermediate cross sections.

## Out-of-plane instability and electron-phonon contribution to ...

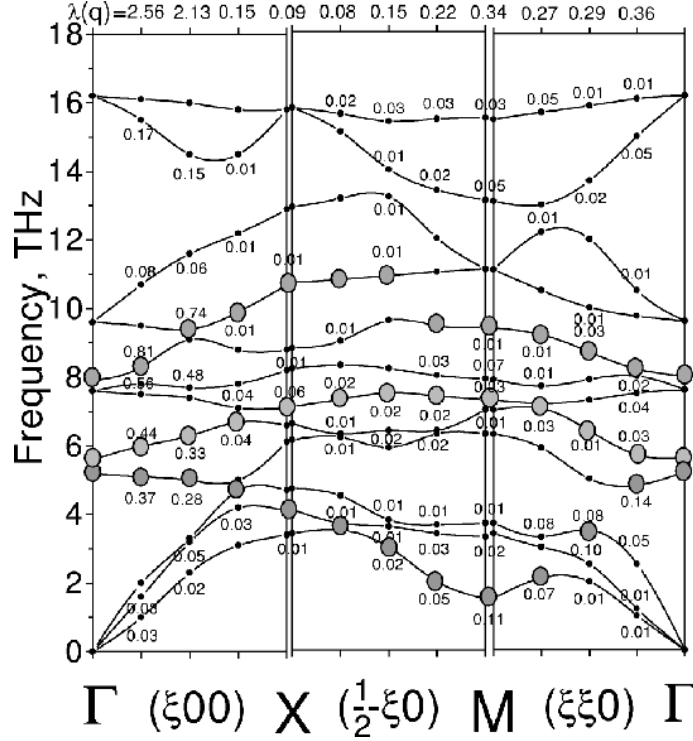


Fig. 5. Calculated phonon spectrum of doped  $\text{CaCuO}_2$  for  $q_z=0$ . Of the branches labelled by solid circles, the lowest is a quadrupolar mode involving in-plane rotation of oxygen squares around Cu and  $z$ -movement of Ca. The two uppermost branches labelled by solid circles involve out-of-plane oxygen buckling. The numbers give the  $s$ -channel mode EPIs,  $\lambda_{s,\nu}(q)$ , and, at the top of the figure, the sum over all modes,  $\lambda_s(q) = \sum_{\nu} \lambda_{s,\nu}(q)$ .

mode exists near the point M. This mode is quadrupolar with the oxygen squares rotated around the copper atoms. It can also be viewed as an in-plane buckling mode and is strongly coupled to the in-plane  $pd\pi$  bands. The mode also involves displacements of the Ca atoms in the  $z$ -direction. It is interesting to note that for the structure with flat planes, this quadrupolar mode is unstable (at M,  $\omega = 3.7i$  THz). This is connected with the atypical feature near point A of the band structure in Fig. 1. Here again we see that, for structural stability of this compound, out-of-plane distortion is required.

### 2.3. Linear electron-phonon interaction

A large amount of theoretical work has been done to estimate the EPI in the cuprates using the frozen-phonon approach,<sup>18,19</sup> the rigid-muffin-

tin,<sup>20</sup> and tight-binding approximations.<sup>21</sup> In addition, there are numerous attempts to deduce the strength of the EPI from experiments.<sup>22</sup> So far, no general agreement is reached, although the LDA frozen-phonon calculations<sup>18,19</sup> for selected, high-symmetry phonons in YBa<sub>2</sub>Cu<sub>3</sub>O<sub>7</sub> and optimally doped La<sub>2</sub>CuO<sub>4</sub> indicate that  $\lambda_s \sim 0.5-1.5$ . Compared herewith, our linear-response method is more accurate because it allows calculation for arbitrary phonon wave vectors  $\mathbf{q}$ . We have checked this method on EPIs for a large number of classical superconductors<sup>16</sup> and the results indicate that, granted the LDA, we can obtain reliable estimates of  $\lambda$  for the high-T<sub>c</sub> materials.

Due to the recent experimental evidence for  $d_{x^2-y^2}$  symmetry of the gap,<sup>2</sup> we have calculated the strength of the EPI in a general  $L$ -channel. We use a standard expression for the mode dependent coupling:

$$\begin{aligned} \lambda_{L,\nu}(\mathbf{q}) &= \frac{1}{\pi N_L} \frac{\gamma_{L,\nu}(\mathbf{q})}{\omega_\nu^2(\mathbf{q})} \\ &\approx \frac{2}{\omega_\nu(\mathbf{q}) N_L} \sum_{\mathbf{k}} \delta(\epsilon(\mathbf{k})) Y_L^*(\hat{\mathbf{k}}) |g_\nu(\mathbf{k}, \mathbf{k} + \mathbf{q})|^2 \\ &\quad \times Y_L(\widehat{\mathbf{k} + \mathbf{q}}) \delta(\epsilon(\mathbf{k} + \mathbf{q})) \end{aligned} \quad (1)$$

where  $\sum_{\mathbf{k}} \equiv \int_{BZ} d^3k/BZV$  is the average over the Brillouin zone,

$$N_L \equiv \sum_{\mathbf{k}} \delta(\epsilon(\mathbf{k})) |Y_L(\hat{\mathbf{k}})|^2 \quad (2)$$

is the electronic ' $L$ -density of states' per spin at the Fermi level ( $\epsilon_F \equiv 0$ ),  $\gamma_{L,\nu}(\mathbf{q})$  is the phonon line-width due to EPI in the  $L$ -channel,  $\omega_\nu(\mathbf{q})$  is the phonon energy, and we have used Rydberg units. For the electronic energies,  $\epsilon_j(\mathbf{k})$ , we have dropped the band index  $j$  because the FS of CaCuO<sub>2</sub> has only one sheet. The approximation in the second line of (1) is, that the bands are linear in the range  $\epsilon_F \pm \omega_\nu(\mathbf{q})$ . This approximation ought to be scrutinized in a future work. Finally, the coupling constant  $\lambda_L \equiv \sum_{\nu\mathbf{q}} \lambda_{L,\nu}(\mathbf{q})$  is the sum over all phonon branches  $\nu$  and the average over the Brillouin zone.

Fig. 5 shows  $\lambda_{s,\nu}(\mathbf{q})$  for the different phonon branches as a function of  $\mathbf{q}$  along high-symmetry directions. The EPI is seen to be particularly large for the buckling modes (the two uppermost of the branches marked by circles). Remember that for flat planes, these contributions to the EPI would vanish. It is furthermore seen that the EPI is strongly enhanced along  $\Gamma X$ , and peaks near  $\Gamma X/3$  reaching a maximum of about 2.5. This is partly due to nesting corresponding to *sliding* of the nearly flat (100)- or (010)-oriented part of the FS on itself, or on the part parallel to it and displaced by  $(0, \frac{\pi}{3a}, 0)$  or  $(\frac{\pi}{3a}, 0, 0)$ , respectively. These sliding-nestings cause



Out-of-plane instability and electron-phonon contribution to ...

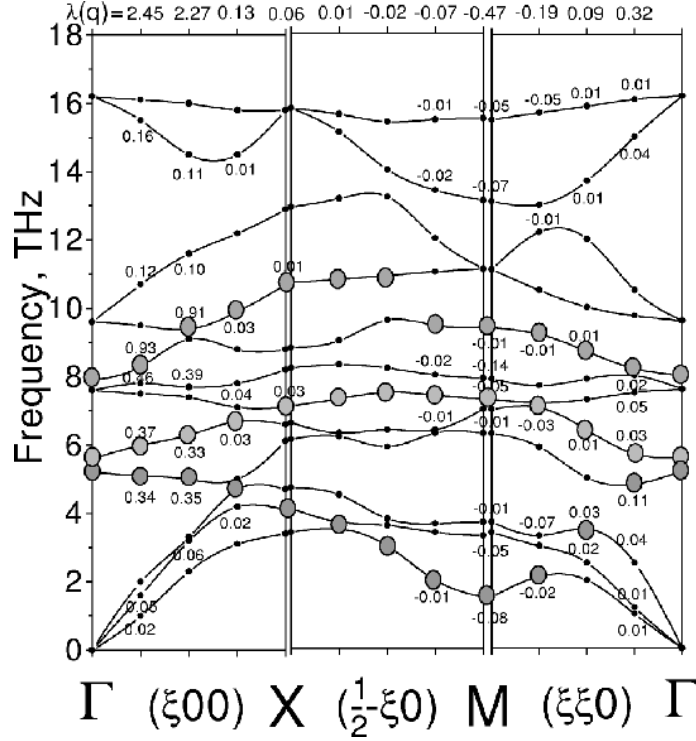


Fig. 6. Contributions to the electron-phonon coupling in the  $d_{x^2-y^2}$ -channel from different phonon branches. See also caption to Fig. 5.

$\sum_{\mathbf{k}} \delta(\epsilon(\mathbf{k})) \delta(\epsilon(\mathbf{k} + \mathbf{q})) \propto \lim_{\omega \rightarrow 0} \chi_0''(\mathbf{q}, \omega) / \omega$  to be large near the following flat regions of  $\mathbf{q}$ -space:  $\mathbf{q} = (q_x, 0, q_z)$ ,  $\mathbf{q} = (0, q_y, q_z)$ ,  $\mathbf{q} = (q_x, \frac{\pi}{3a}, q_z)$  and  $\mathbf{q} = (\frac{\pi}{3a}, q_y, q_z)$ , with  $q_x$  and  $q_y$  considerably smaller than  $\frac{\pi}{a}$  and  $q_z$  considerably smaller than  $\frac{\pi}{c}$ . This kind of nesting enhancement is well-known in the theory of HTSC.<sup>23</sup> A second reason for the peaking of  $\lambda_{s,\nu}(\mathbf{q})$  near  $\Gamma X/3$  is a particular wave-vector dependence the EP coupling constants  $g_\nu(\mathbf{k}, \mathbf{k} + \mathbf{q})$  for the buckling modes; this we shall return to in the next section where we consider the tight-binding model. From Fig. 5 we see that the EPI is small in other points of the Brillouin Zone. Averaging over 15  $\mathbf{q}$ -points in the  $\Gamma XM$ -plane yields:  $\lambda_s(q_z=0) = 0.5$ , and averaging over the ZRA-plane gives:  $\lambda_s(q_z=\frac{\pi}{c}) = 0.2$ . These values are respectively upper and lower bounds for  $\lambda_s$  averaged over all  $\mathbf{q}$ . We conclude that  $\lambda_s \sim 0.4$  is too small to account for the high-temperature superconductivity in doped  $\text{CaCuO}_2$ .

Finally, we discuss our calculation of the  $d$ -channel EPIs. Using eqs. (1-2) we have analyzed all symmetry-allowed channels of superconductivity and came to the conclusion that, apart from the  $s$ -channel, relatively large positive values of  $\lambda_L$  are only obtained for pair-function symmetry  $d_{x^2-y^2}$ .

Note that if  $g$  were a constant, independent of  $\mathbf{k}$  and  $\mathbf{q}$ ,  $\lambda_L$  would vanish for  $L \neq 0$ . The  $\lambda_{x^2-y^2,v}(\mathbf{q})$  are presented in Fig. 6 and may be compared with  $\lambda_{s,\nu}(\mathbf{q})$  in Fig. 5. Also for  $\lambda_{x^2-y^2,v}(\mathbf{q})$  there is a strong enhancement near  $\Gamma X/3$  and, in particular, for the buckling modes. It is also seen that near the M-point,  $\lambda_{x^2-y^2,v}(\mathbf{q})$  vanishes for the buckling modes and is negative for all other modes. Averaging over  $\mathbf{q}$  in the  $\Gamma XM$  and ZRA planes give respectively:  $\lambda_{x^2-y^2}(q_z=0) = 0.4$  and  $\lambda_{x^2-y^2}(q_z=\frac{\pi}{c}) = 0.2$ . These values are *positive* and only *slightly smaller* than the corresponding values of  $\lambda_s$ . The electron-phonon coupling is thus *highly anisotropic* in 24 per cent hole-doped CaCuO<sub>2</sub>, and probably in all HTSCs near optimal doping.

### 3. ANALYTICAL MODEL

#### 3.1. Electronic 8-band Hamiltonian

In the bottom part of Fig. 7 we specify an electronic 8-band orthogonal tight-binding Hamiltonian for a single, dimpled CuO<sub>2</sub> plane, which we feel is generic for CuO<sub>2</sub>-HTSC's and contains the relevant degrees of freedom. In the upper part, we synthesize the eight plane-bands. This Hamiltonian was originally<sup>8</sup> derived from the LDA bands of YBa<sub>2</sub>Cu<sub>3</sub>O<sub>7</sub> by integrating out the very-high-energy degrees of freedom, neglecting the chains, and projecting onto one plane (or, for a bi-layer, to the even or the odd linear-combination, or, for an infinite-layer, to a single  $k_z$ ).<sup>9</sup> We have recently<sup>24</sup> deduced the parameter values of this Hamiltonian for a number of further HTSC's and showed that (apart from Fermi-level position) the only strongly material-dependent parameters are the energy  $\epsilon_s$  of the Cu <sub>$s-(3z^2-1)$</sub>  hybrid,<sup>9</sup> which depends on the distance of apical oxygen from plane copper, and the integral of hopping  $t_{zd}$  from the Cu <sub>$x^2-y^2$</sub>  orbital to an O <sub>$z$</sub>  orbital, which is proportional to the buckling-angle  $\delta$ . For simplicity, we assume tetragonal symmetry in Fig.7 as well as in most of the following. For a discussion of the inter-plane hopping, we refer to Ref.<sup>9</sup>

Shown in the 2nd row and 1st column of Fig. 7, which we shall refer to as Fig. 7(2,1), are the four  $\sigma$ -orbitals looked upon from above the plane,  $|y\rangle \equiv O_y$ ,  $|d\rangle \equiv \text{Cu}_{x^2-y^2}$ ,  $|x\rangle \equiv O_x$ , and  $|s\rangle \equiv \text{Cu}_{s-(3z^2-1)}$ . Note that O <sub>$y$</sub>  and O <sub>$x$</sub>  refer to orbitals on two different oxygens, O2 at  $(1, 0, \tan \delta)a/2$  and O3 at  $(0, 1, \tan \delta)a/2$ . For some purposes, we shall also distinguish the two oxygens by labels  $a$  and  $b$ . In Fig. 7(3,1), we see the  $|d\rangle$  orbital and two of the  $\pi$ -orbitals,  $|z\rangle \equiv O_z$  and  $|xz\rangle \equiv \text{Cu}_{xz}$  from the edge of the plane. Approximate orbital energies (in eV and with respect to the energy of the Cu <sub>$x^2-y^2$</sub>  orbital) are given at the relevant points of the band structure shown above, in Fig.7(1,1). Hence,  $\epsilon_x=\epsilon_y \equiv \epsilon_p$  is 0.9 eV *below*  $\epsilon_d$ , and  $\epsilon_s$  is 6.5 eV above. Moreover,  $\epsilon_{za}=\epsilon_{zb} \equiv \epsilon_z$  is 0.4 eV above  $\epsilon_d$ , and  $\epsilon_{xz}=\epsilon_{yz}$  is 1 eV

Out-of-plane instability and electron-phonon contribution to ...

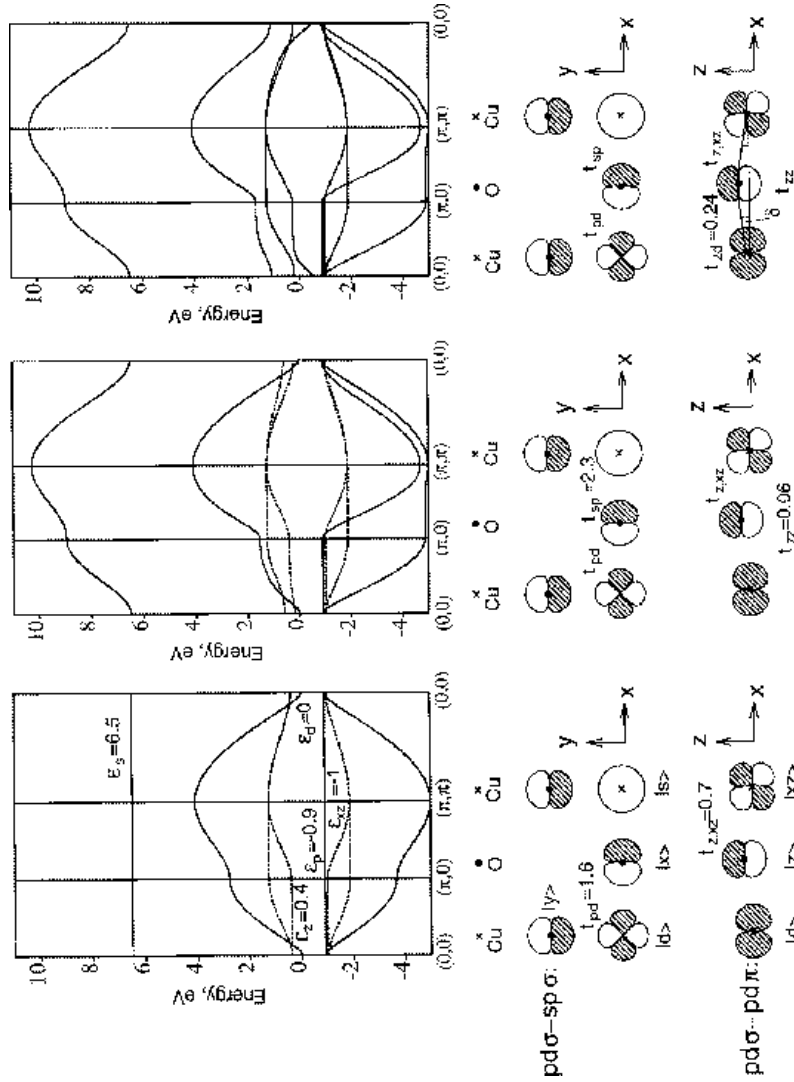


Fig. 7. The 8-band Hamiltonian for a single  $\text{CuO}_2$  plane and synthesis of its band structure. The 1st (left) column shows uncoupled  $pd\sigma$  ( $O_x$ - $\text{Cu}_{x^2-y^2}$ - $O_y$ ),  $\text{Cu}_s$ , and  $pd\pi$  ( $\text{Cu}_{xz}$ - $O_z$  and  $\text{Cu}_{yz}$ - $O_z$ , stippled) bands. In the 2nd (middle) column, the coupling ( $t_{sp}$ ) of the  $\text{Cu}_s$  orbital to the  $pd\sigma$  band has been included. In the 3rd (right) column, also the coupling ( $t_{zd}$ ) between  $\sigma$ - and  $\pi$ -bands has been included. All energies are in eV.

below. If we now, as shown in Figs. 7 (2,1) and (3,1) include the  $pd\sigma$  hopping integrals  $t_{xd}=t_{yd} \equiv t_{pd}=1.6$  eV and the  $pd\pi$  hopping integrals  $t_{z,xz}=t_{z,yz}=0.7$  eV, we obtain the band structure shown in Fig. 7(1,1): The  $\sigma$ -orbitals give rise to a bonding, a non-bonding, and an anti-bonding  $O_x-Cu_{x^2-y^2}-O_y$  band plus a  $Cu_{s-(3z^2-1)}$  level (full lines), and the  $\pi$ -orbitals give rise to two decoupled pairs of bonding anti-bonding bands which disperse in either the  $x$  or  $y$  direction (stippled lines). The anti-bonding  $pd\sigma$  band, which will develop into the conduction band, has saddle-points at X (and Y) which are well above the top of the  $\pi$ -bands, and which are *isotropic* in the sense, that the absolute values of the band masses in the  $x$  and  $y$  directions are equal. This means that the FS at half-filling is a square with corners at X and Y. This is shown in Fig. 8(1,1).

In the 2nd columns of Figs. 7 and 8, the  $\sigma$  and  $\pi$  bands remain decoupled, but we have introduced the  $Cu_s-O_x$  and  $Cu_s-O_y$  hoppings ( $t_{sp}=2.3$  eV), as well as the tiny  $O_z-O_z$  hopping ( $t_{zz}=0.06$  eV). The latter is the only one reaching beyond nearest neighbors and it merely lifts a degeneracy of the anti-bonding  $\pi$ -bands at  $\Gamma$ . We shall neglect it in the following. The *strong* coupling of the *remote*  $Cu_{s-(3z^2-1)}$  orbital to the  $pd\sigma$  orbitals has the pronounced effect of depressing the conduction band near the saddle-points at X and Y, and thereby increasing the mass towards  $\Gamma$  and decreasing it towards M ( $\pi, \pi$ ). This kind of saddle-point we refer to as *anisotropic*. As seen in Fig. 8(1,2), the FS passing through X and Y will therefore correspond to a finite hole-doping and will bulge towards  $\Gamma$ . That the  $Cu_{s-(3z^2-1)}$  orbital, which has the azimuthal quantum number  $m_z=0$ , may mix with the conduction band at X (and Y), but not along  $\Gamma M$  follows from the symmetries of the corresponding two antibonding  $pd\sigma$  wave functions.<sup>9</sup> The net downwards shift of the saddle-point energy is the result of down-pushing by  $Cu_s$  and weak up-pushing by  $Cu_{3z^2-1}$ , whose energy is below the saddle-point.

As a result of the hybridization with the  $Cu_{s-(3z^2-1)}$  orbital, the saddle-points of the anti-bonding  $\sigma$ -band straddle off the top of the appropriate  $\pi$ -band, so that even a weak dimple or buckle of the planes will introduce noticeable hybridization between the  $\sigma$  and  $\pi$  bands. This is seen in the 3rd column of Fig. 7 where we have turned on the weak  $Cu_{x^2-y^2}-O_z$  hoppings ( $t_{zd}=0.24$  eV  $\propto \sin \delta$ ). These couplings become allowed when there is a finite angle  $\delta$  ( $\approx 7^\circ$  in  $YBa_2Cu_3O_7$ ,  $YBa_2Cu_4O_8$ , and in calculated  $CaCuO_2$ ) between the Cu-O bond and the plane of the 2D-translations. Since the hybridization between the antibonding  $pd\sigma$  and  $Cu_{xz}-O_z$   $pd\pi$  orbitals vanish at X (along the XM-line), the  $\sigma$ - $\pi$  hybridization may make the saddle-point *bifurcate* away from X. This is seen in Fig. 8(1,3). At X (along XM), the  $pd\sigma$ -band does hybridize with the more remote  $Cu_{yz}-O_z$   $pd\pi$  band.

## Out-of-plane instability and electron-phonon contribution to ...

### 3.2. Constant-energy contours (CECs)

The orbitals in the Bloch representation and the 8-band Hamiltonian may be found in eq.(2) of Ref.<sup>8</sup> and in eq.(1) of Ref.<sup>9</sup> As shown in the former reference, and given explicitly in its eqs.(12-16), the constant-energy contours (CECs),  $\epsilon_j(\mathbf{k}) = \epsilon$ , have simple analytical expressions. These are given in the 3rd and 4th rows of Fig. 8 in order of increasing couplings as in Fig. 7. In the present paper we shall neglect the  $\text{Cu}_{xz}$  and  $\text{Cu}_{yz}$  orbitals and, hence, consider the 6- rather than the 8-band Model (this corresponds to using eq.(14) in Ref.<sup>8</sup>), because then the CECs are just hyperbolas in  $(x, y)$ -space, where

$$x \equiv \frac{1}{2}(1 - \cos ak_x) \quad \text{and} \quad y \equiv \frac{1}{2}(1 - \cos ak_y), \quad (3)$$

and they are shown in the 2nd row of Fig. 8. A CEC is specified by 3 numbers  $d$ ,  $s$ , and  $p$ , which are the values of the scattering functions defined in the 4th row of Fig. 8.  $d(\epsilon)$  specifies the  $pd\sigma$  interaction,  $s(\epsilon)$  the  $sp\sigma$  interaction, and  $p(\epsilon)$  the  $\sigma\pi$  interaction. Only  $d(\epsilon)$  has a non-negligible (increasing) energy-dependence in the relevant  $\pm 0.1$  eV range around  $\epsilon_F$ . For isotropic saddlepoints,  $s \rightarrow \infty$ , and for the cases of interest,  $s \sim 0.5 - 1.5$ . For a flat plane,  $p = 0$ . If  $p = s^2/(1 + s)^2$ , the saddlepoint is *extended*, that is, the dispersion is quadratic towards M, but *quartic* towards  $\Gamma$ . If  $p$  exceeds this value, the saddlepoint bifurcates to the positions given by  $x = s(p^{-1/2} - 1)$  and  $y = 0$ . It should be noted that, although the CECs near  $\epsilon_F$  can be well reproduced by the 6-band model with an energy-independent  $p$ , because  $\epsilon_{xz} = \epsilon_{yz}$  are several eV below  $\epsilon_F$  and 1.4 eV below  $\epsilon_{za} = \epsilon_{zb}$ , the value of  $p$  should be adjusted to give the correct CECs.

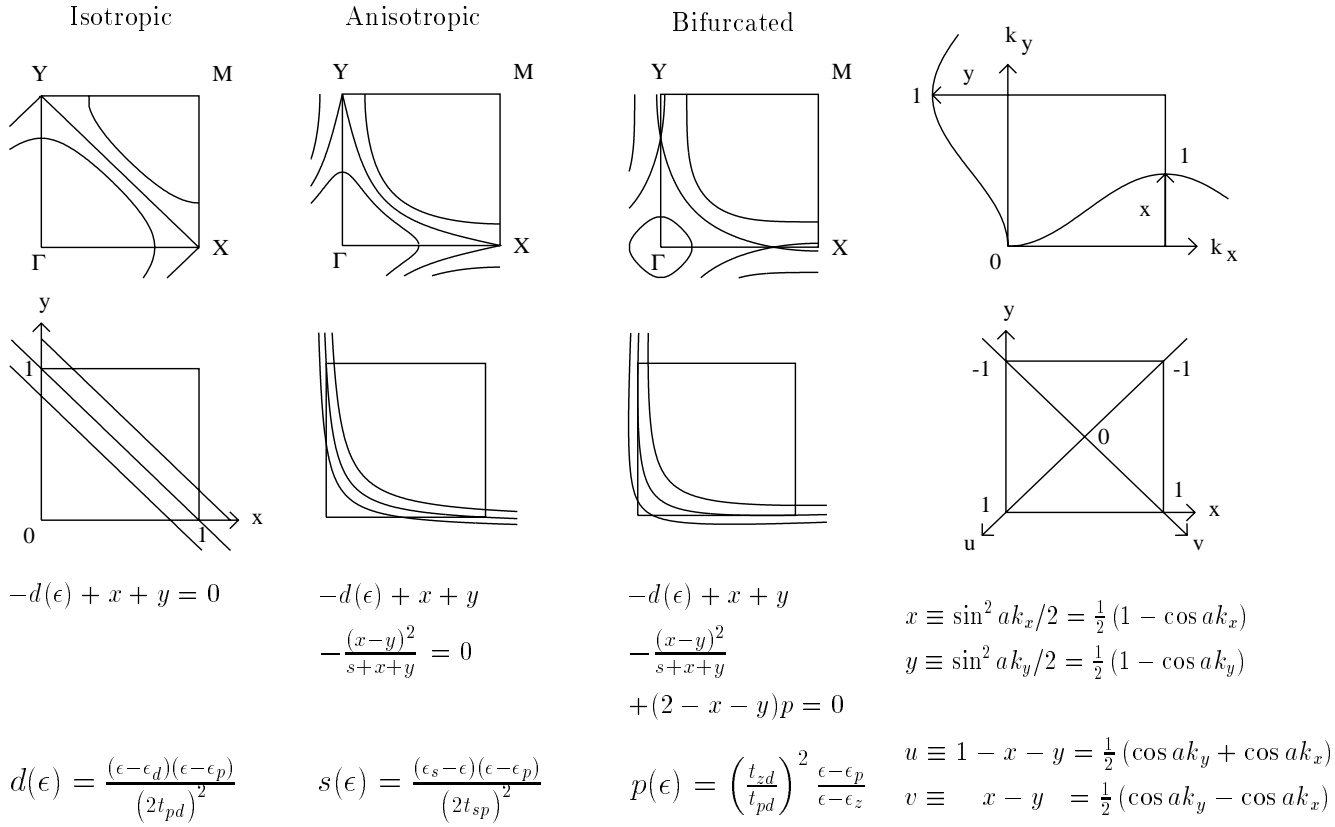
The structure of  $\chi_0''(\mathbf{q}, \omega)$  obtained from the 6-band model as functions of doping,  $s$ , and  $p$  is discussed in Ref.<sup>25</sup>

The formalism given above is for tetragonal symmetry and apparently only applies to a plane dimpled like in  $\text{YBa}_2\text{Cu}_3\text{O}_7$ , but not to a plane buckled as in Fig. 2. However, since in the 6-band model each  $\text{O}_z$ -orbital couples only to the  $\text{Cu}_{x^2-y^2}$ -orbital, we can freely define the sign of the  $\text{O}_z$  orbital at  $(1, 0, \tan \delta)a/2, |za\rangle$ , to be the opposite of that at  $(0, 1, -\tan \delta)a/2, |zb\rangle$ , and then the formalism holds also for static buckling. Nevertheless, for the sake of preciseness in the wording, we shall assume static dimpling in the following. The values of the electronic parameters for various materials may be found in Ref.<sup>24</sup>

In  $(x, y)$ -space the average over the Brillouin zone becomes:

$$\sum_{\mathbf{k}} \equiv \left(\frac{a}{2\pi}\right)^2 \int_{-\pi/a}^{\pi/a} \int_{-\pi/a}^{\pi/a} dk_x dk_y = \left(\frac{1}{\pi}\right)^2 \int_0^1 \int_0^1 \frac{dx dy}{\sqrt{xy(1-x)(1-y)}}. \quad (4)$$

Fig. 8. Caption is given at the next page.



### Out-of-plane instability and electron-phonon contribution to ...

CAPTION to Fig. 8. The top row of the first three columns shows CECs in  $(k_x, k_y)$ -space of the 8-band Hamiltonian corresponding to the three columns in Fig. 7. The CECs chosen in the figures are antibonding  $pd\sigma$ -like and are, specifically, the one passing through the saddle-point ( $\epsilon \equiv \epsilon_{\text{saddle}}$ ) and two neighboring ones ( $\epsilon \equiv \epsilon_{\text{saddle}} \pm \Delta\epsilon$ ). The 4th column illustrates the transformation from  $(k_x, k_y)$ -space to  $(x, y)$ -, or  $(u, v)$ -, space. The 2nd row shows the CECs in  $(x, y)$ -space where they are hyperbolas. The 3rd row gives the expressions for the CECs and the  $(k_x, k_y)$ - $(x, y)$  transformation. The 4th row gives the expressions for the scattering functions, and the  $(u, v)$ - $(x, y)$ transformations. For simplicity, the CECs in the 3rd column are for the 6-band Hamiltonian where, of the  $\pi$ -orbitals, only the two  $O_z$ -orbitals and not the  $\text{Cu}_{zx}$ - and  $\text{Cu}_{yz}$ -orbitals are included.

### 3.3. Coupling of electrons to the buckling mode

The displacement pattern of the buckling mode is:

$$\left\{ \frac{\partial \mathbf{R}_{O2}}{\partial Q_{\mathbf{q}}}, \frac{\partial \mathbf{R}_{O3}}{\partial Q_{\mathbf{q}}} \right\} = \frac{\hat{\mathbf{z}}}{\sqrt{2M\omega}} \frac{1}{\sqrt{2}} \{ \exp(-i\mathbf{q} \cdot \mathbf{R}_{O2}), -\exp(-i\mathbf{q} \cdot \mathbf{R}_{O3}) \} \quad (5)$$

where O2 and O3 are the oxygens at respectively  $(1, 0, \tan \delta)a/2$  and  $(0, 1, \tan \delta)a/2$  and  $\mathbf{q}$  is 2-dimensional.

For  $\mathbf{q} = \mathbf{0}$ , this is the mode for which the dimple of O2 is increased and that of O3 is decreased, or vice versa. For  $\text{YBa}_2\text{Cu}_3\text{O}_7$ , this is the 330  $\text{cm}^{-1}$  out-of-phase mode. Had  $\delta$  been zero at equilibrium, oxygen would have been dimpling upwards in the  $-\text{Cu}-\text{O}_2-\text{Cu}-$  rows and downwards in the  $-\text{Cu}-\text{O}_3-\text{Cu}-$  rows, that is what we have called buckling.

$\mathbf{q} = (\frac{\pi}{a}, 0)$  : Had  $\delta$  been zero at equilibrium, this mode would have been buckling in the  $x$ -direction and dimpling in the  $y$ -direction.

$\mathbf{q} = (\frac{\pi}{a}, \frac{\pi}{a})$  : Had  $\delta$  been zero at equilibrium, both the  $-\text{Cu}-\text{O}_2-\text{Cu}-$  and the  $-\text{Cu}-\text{O}_3-\text{Cu}-$  rows would be buckling, and such that the  $\text{O}_2-\text{O}_3-\text{O}_2$ -rows in the  $x=y$  direction are in phase. This is the displacement pattern of the low-temperature orthorhombic (LTO) phase in  $\text{La}_2\text{CuO}_4$ .

For this mode, the electron-phonon matrix element is:

$$\begin{aligned} g(\mathbf{k}, \mathbf{k}' \equiv \mathbf{k} + \mathbf{q}) &= \\ &= \frac{1}{\sqrt{2M\omega}} \langle \mathbf{k} | \sum_{\mathbf{R}} \frac{1}{\sqrt{2}} \left( \frac{\partial H}{\partial z_{O2}} \exp(-i\mathbf{q} \cdot \mathbf{R}_{O2}) - \frac{\partial H}{\partial z_{O3}} \exp(-i\mathbf{q} \cdot \mathbf{R}_{O3}) \right) | \mathbf{k}' \rangle \\ &= \frac{\partial t_{zd}/\partial z_O}{\sqrt{M\omega}} \left[ \begin{aligned} &c_d(\mathbf{k}) (\cos \frac{a}{2} k_x |c_a(\mathbf{k}')| - \cos \frac{a}{2} k_y |c_b(\mathbf{k}')|) + \\ &\text{sgn} \{c_a(\mathbf{k}') c_a(\mathbf{k})\} \left( |c_a(\mathbf{k})| \cos \frac{a}{2} k'_x - |c_b(\mathbf{k})| \cos \frac{a}{2} k'_y \right) c_d(\mathbf{k}') \end{aligned} \right] \end{aligned}$$

where, for simplicity, we have only included the phonon-induced modulation of the hopping integral  $t_{zd}$ . The modulation of  $\epsilon_z$  due to screening is considered in Ref.<sup>24</sup> The eigenvector-components,  $c_d(\mathbf{k})$ ,  $c_a(\mathbf{k})$ , and  $c_b(\mathbf{k})$ , for the Bloch orbitals  $|d, \mathbf{k}\rangle$ ,  $|za, \mathbf{k}\rangle$  and  $|zb, \mathbf{k}\rangle$  are real due to our choice of phases for the Bloch functions, and they are most easily obtained by differentiation of the CEC-equation with respect to the orbital energies,  $\epsilon_d$ ,  $\epsilon_{za}$ , and  $\epsilon_{zb}$ . According to first order perturbation theory, this yields  $c_d(\mathbf{k})^2 = \partial\epsilon(\mathbf{k})/\partial\epsilon_d$ , and so on. Simple considerations finally yield the relative signs. As a result, we obtain by using the 6-band model:

$$\begin{aligned}
 g(\mathbf{k}, \mathbf{k}') &= 2t_{zd} \frac{\epsilon_F - \epsilon_p}{(\epsilon_F - \epsilon_z) \left(\epsilon_F - \frac{\epsilon_p + \epsilon_d}{2}\right)} \frac{\partial t_{zd}/\partial z_O}{\sqrt{M\omega}} \times \\
 &\quad \left( \left| \cos \frac{a}{2} k_x \cos \frac{a}{2} k'_x \right| - \left| \cos \frac{a}{2} k_y \cos \frac{a}{2} k'_y \right| \right) \\
 &= c \left( \sqrt{(1-x)(1-x')} - \sqrt{(1-y)(1-y')} \right). \tag{6}
 \end{aligned}$$

where  $c$  is the constant in front of the parenthesis on the first line.

In order to get a feeling for the behavior of the pair-interaction,  $V \propto -g^2$ , let us first take  $\mathbf{q} = \mathbf{0}$ , i.e.  $\mathbf{k}' = \mathbf{k}$ . Eq.(6) then yields:  $g = c(y - x)$  which shows that  $g^2$  attains its maximum ( $c^2$ ) for  $\mathbf{q}$  small and  $\mathbf{k}$  at those points of the FS where the density of states (distance between neighboring CECs) is largest and where the superconducting gap is observed to be largest. That is, near the saddlepoints.

Next, let us take  $\mathbf{k}'$  at the X-point,  $[x', y'] = [1, 0]$ . Then,  $g = c\sqrt{1-y}$ . We thus see that not only does  $g^2$  take its *maximal* value for  $\mathbf{k} = \mathbf{k}'$  at X, but it *vanishes* for  $\mathbf{k}$  at X and  $\mathbf{k}'$  at Y. This is exactly what is needed for the electron-phonon interaction to support  $d_{x^2-y^2}$ -pairing.

Finally, let  $\mathbf{k}$  and  $\mathbf{k}'$  to be symmetric around the (1, 1) or (1, -1) line, i.e.  $(k'_x, k'_y) = (\pm k_y, \pm k_x)$ , in which case  $\mathbf{q}$  is in the (1,  $\mp$ 1) direction. In this case,  $g = V = 0$ . In particular, this means that  $V$  vanishes for  $\mathbf{q} = (\frac{\pi}{a}, \frac{\pi}{a})$  where the Coulomb repulsion is maximal.

Having realized that the buckling mode has the right kind of  $(\mathbf{k}, \mathbf{k}')$ -dependence to support  $d_{x^2-y^2}$ -wave pairing, let us calculate  $\lambda_{x^2-y^2}$  for the buckling mode and see whether it is really positive. For this purpose we note that

$$\begin{aligned}
 g^2(\mathbf{k}, \mathbf{k}') &= c^2 \times \\
 &\quad \left[ (1-x)(1-x') + (1-y)(1-y') - 2\sqrt{(1-x)(1-y)(1-x')(1-y')} \right]
 \end{aligned}$$



### Out-of-plane instability and electron-phonon contribution to ...

is factorized so that we can easily calculate  $\lambda_L \equiv \sum_{\mathbf{q}} \lambda_L(\mathbf{q})$  as a double-integral, not over  $\mathbf{k}$  and  $\mathbf{q}$  as in (1), but over  $\mathbf{k}$  and  $\mathbf{k}'$ . Dropping the  $\mathbf{q}$ -dependence of the buckling-mode frequency, we get using (4):

$$\lambda_s = \frac{4c^2}{\pi^2\omega} \times \frac{\left[ \int_0^1 \int_0^1 (1-x) \delta(\epsilon) \frac{dxdy}{\sqrt{xy(1-x)(1-y)}} \right]^2 - \left[ \int_0^1 \int_0^1 \delta(\epsilon) \frac{dxdy}{\sqrt{xy}} \right]^2}{\int_0^1 \int_0^1 \delta(\epsilon) \frac{dxdy}{\sqrt{xy(1-x)(1-y)}}}$$

where  $\delta(\epsilon) \equiv \delta(\epsilon(x, y) - \epsilon_F)$ . Using  $Y_{x^2-y^2}(\mathbf{k}) \propto x - y$  we get:

$$\lambda_d = \frac{4c^2}{\pi^2\omega} \times \frac{\left[ \int_0^1 \int_0^1 (1-x)(x-y) \delta(\epsilon) \frac{dxdy}{\sqrt{xy(1-x)(1-y)}} \right]^2 - \left[ \int_0^1 \int_0^1 (x-y) \delta(\epsilon) \frac{dxdy}{\sqrt{xy}} \right]^2}{\int_0^1 \int_0^1 (x-y)^2 \delta(\epsilon) \frac{dxdy}{\sqrt{xy(1-x)(1-y)}}}.$$

Now, the last term of  $\lambda_d$  vanishes and we may symmetrize the first term as follows:  $(1-x)(x-y) \rightarrow \frac{1}{2}[(1-x)(x-y) + (1-y)(y-x)] = -\frac{1}{2}(x-y)^2$ . As a result:

$$\lambda_d = \frac{c^2}{\pi^2\omega} \int_0^1 \int_0^1 (x-y)^2 \delta(\epsilon(x, y)) \frac{dxdy}{\sqrt{xy(1-x)(1-y)}} = \frac{c^2}{\omega} N_d \quad (7)$$

which is *positive*, and easy to evaluate.

It is obvious from these equations, that if the FS had weight merely at X and Y, that is, if  $\epsilon_F$  were at a non-bifurcated saddlepoint, then

$$\lambda_s = \lambda_d \ (\rightarrow \infty).$$

For  $\epsilon_F$  near an extended saddlepoint,  $\lambda_d$  is particularly large.

The integral (7), as well as the one for the normal density of states,  $N \equiv N_s$ , may be expressed analytically in terms of elliptic integrals if we use a band structure with  $p = 0$ , i.e. the 4-band model. The results for  $s = 100$  and  $s = 0.6$  are shown graphically in Fig. 9 as a functions of the doping. We see that for doping to the van Hove singularity,  $N_d = N$ , as was stated above.

## 4. CONCLUSIONS

We conclude that the linear electron-phonon interaction for buckled planes may support, but is hardly sufficient to cause, high-temperature superconductivity based on  $d_{x^2-y^2}$ -pairing. The most important mode seems

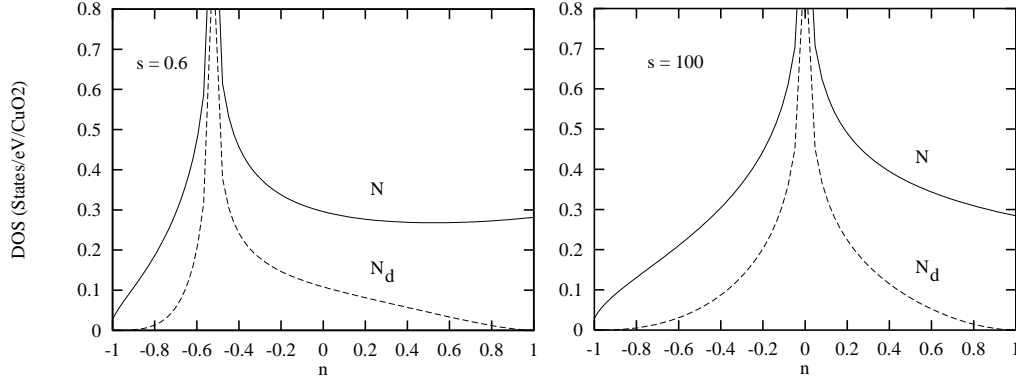


Fig. 9. Density of states and  $d_{x^2-y^2}$  weighted density of states as defined in eq. 2 for the 4-band model.  $n$  is the number of electrons counted from the half-full band.

to be the buckling mode, because it modulates the saddlepoints of the energy bands where the density of states is high and where the superconducting gap is observed to be maximum. Moreover, the buckling mode does not interact with the electrons for  $\mathbf{q}$  near  $(\frac{\pi}{a}, \frac{\pi}{a})$  where the Coulomb repulsion is maximum.

Considering the facts that the linear EPI for the buckling mode is proportional to the small static (on the scale of phonon frequencies) buckling, and that this mode is calculated to be highly anharmonic, it seems imminent to investigate the role of anharmonicity. Similarly, the interplay between the electron-phonon interaction and the Coulomb repulsion should be studied. For these purposes the analytical 6-band models seem realistic and tractable.

## ACKNOWLEDGMENTS

The authors are indebted to M. Kulić, E. G. Maksimov, I. I. Mazin, and R. Zeyer for many helpful discussions.

## REFERENCES

1. For a recent review, see, *e.g.*, N. M. Plakida, *High-Temperature Superconductivity* (Springer-Verlag, Berlin, 1995).
2. For a recent review, see, *e.g.*, D. J. Scalapino, Phys. Rep. **250**, 329 (1995).
3. C. Thomsen and M. Cardona, in *Physical Properties of High-Temperature Superconductors I*, ed. by D. M. Ginsberg (World Scientific, Singapore, 1989), p. 409.
4. C. Frank, in *Physical Properties of High-Temperature Superconductors IV*, ed. by D. M. Ginsberg (World Scientific, Singapore, 1993), p. 189.

### Out-of-plane instability and electron-phonon contribution to ...

5. S. I. Vedeneev, P. Samuely, S. V. Meshkov, G. M. Eliashberg, A. G. M. Jansen, P. Wyder, *Physica C* **198**, 47 (1992); N. Miyakawa, Y. Shiina, T. Kaneko, N. Tsuda, *J. Phys. Soc. Jpn.* **62**, 2445 (1993).
6. M. Azuma, Z. Hirori, M. Takano, Y. Bando, Y. Takeda, *Nature (London)* **356**, 775 (1992).
7. H. Shaked, Y. Shimakawa, B. A. Hunter, R. L. Hitterman, J. D. Jorgensen, P. D. Han, D. A. Payne, *Phys. Rev. B* **51**, 11784 (1995). Note, however, that in a publication of J. Karpinski, H. Schwer, I. Mangelschots, K. Conder, A. Morawski, T. Lada, A. Paszewin, *Physica C* **234**, 10 (1994), growth of single crystals of  $Ca_{1-x}CuO_2$  ( $0.01 < x < 0.02$ ) with  $T_c = 70 - 100K$  without stabilizing additives of *Sr* or *Li* in a high-pressure gas system has been reported.
8. O. K. Andersen, O. Jepsen, A. I. Liechtenstein, and I. I. Mazin, *Phys. Rev. B* **49**, 4145 (1994).
9. O. K. Andersen, A. I. Liechtenstein, O. Jepsen, and F. Poulsen, *J. Phys. Chem. Solids* **12**, 1573 (1995).
10. H. Monien, (this volume)
11. S. Chakravarty, A. Sudbø, P.W. Anderson, and S. Strong, *Science* **291**, 337 (1993).
12. D. L. Novikov, V. A. Gubanov, A. J. Freeman, *Physica C* **210**, 301 (1993); B. K. Agrawal, S. Agrawal, *Phys. Rev. B* **48**, 6451 (1993); R. Weht, C. O. Rodriguez, M. Weissmann, *Physica C* **223**, 339 (1994).
13. J.M. Tranquada, B.J. Sternlieb, J.D. Axe, Y. Nakamura, and S. Ushida, *Nature* **375**, 561 (1995).
14. A. Bianconi, N. L. Saini, A. Lanzara, M. Missori, T. Rossetti, H. Oyanagi, H. Yamaguchi, K. Oka, T. Ito, *Phys. Rev. Lett.* **76**, 3412 (1996).
15. S. Y. Savrasov, *Phys. Rev. Lett.* **69**, 2819 (1992); *ibid.*, *Phys. Rev. B* (in press).
16. S. Y. Savrasov, D. Y. Savrasov, O. K. Andersen, *Phys. Rev. Lett.* **72**, 372 (1994); *ibid.*, *Phys. Rev. B* (in press).
17. S. Y. Savrasov and O. K. Andersen (*Phys. Rev. Lett.* submitted).
18. R. E. Cohen, W. E. Pickett, H. Krakauer, *Phys. Rev. Lett.* **64**, 2575 (1990); W. E. Pickett, R. E. Cohen, H. Krakauer, *Phys. Rev. Lett.* **67**, 228 (1991).
19. O. K. Andersen, A. I. Liechtenstein, O. Rodriguez, I. I. Mazin, O. Jepsen, V. P. Antropov, O. Gunnarsson, S. Gopalan, *Physica C* **185-189**, 147 (1991); I. I. Mazin *et. al.*, in *Lattice Effects in High- $T_C$  Superconductors*. Eds. Y. Bar-Yam et al. (World Scientific, 1992).
20. See, *e.g.*, I. I. Mazin, S. N. Rashkeev, S. Y. Savrasov, *Phys. Rev. B* **42**, 366 (1990).
21. G. L. Zhao and J. Callaway, *Phys. Rev. B* **50**, 9511 (1994).
22. See, *e.g.*, P. B. Allen, W. E. Pickett, H. Krakauer, *Phys. Rev. B* **37**, 7482 (1989); R. Zeyher, *Phys. Rev. B* **44**, 10404 (1991); I. I. Mazin, O. V. Dolgov, *Phys. Rev. B* **45**, 2509 (1992); C. T. Rieck, W. A. Little, J. Ruvalds, A. Virosztek, *Phys. Rev. B* **51**, 3772 (1995); F. Marsiglio, J. P. Carbotte, *Phys. Rev. B* **52**, 16192 (1995).
23. H. Krakauer, W. E. Pickett, R. E. Cohen, *Phys. Rev. B* **47**, 1002 (1993).
24. I. Dasgupta, O. Jepsen, and O.K. Andersen (to be published).
25. O.K. Andersen and O. Jepsen (to be published).